Science of the Total Environment 470–471 (2014) 270–281

Contents lists available at ScienceDirect

Science of the Total Environment

journal homepage: www.elsevier.com/locate/scitotenv

Simulated air quality and pollutant budgets over Europe in 2008

U. Im [a,b,1], N. Daskalakis [a,b], K. Markakis [c], M. Vrekoussis [d,e], J. Hjorth [f], S. Myriokefalitakis [a], E. Gerasopoulos [g], G. Kouvarakis [a], A. Richter [h], J. Burrows [h], L. Pozzoli [i], A. Unal [i], T. Kindap [i], M. Kanakidou [a,*]

[a] Environmental Chemical Processes Laboratory, Department of Chemistry, University of Crete, Heraklion, Greece
[b] Institute of Chemical Engineering Sciences, Foundation for Research and Technology Hellas (FORTH/ICE-HT), Patras, Greece
[c] Laboratoire de Meteorologie Dynamique (LMD), IPSL Ecole Polytechnique, Palaiseau Cedex, Paris, France
[d] Energy, Environment and Water Research Center, The Cyprus Institute, Nicosia, Cyprus
[e] Academy of Athens, Athens, Greece
[f] Air and Climate Unit, Joint Research Centre, Ispra, Italy
[g] Institute for Environmental Research and Sustainable Development, National Observatory of Athens, Athens, Greece
[h] Institute of Environmental Physics, University of Bremen, Bremen, Germany
[i] Eurasia Institute of Earth Sciences, Istanbul Technical University, Istanbul, Turkey

HIGHLIGHTS

- Major pollutant levels are simulated over Europe for the year 2008.
- Ozone levels are overestimated while aerosol levels are underestimated.
- Updated emissions over East Mediterranean result in better agreement with observations.
- Emission distributions and photochemistry lead to a north–south gradient.
- Surface ozone is affected by transport from upper troposphere over Europe

ARTICLE INFO

Article history:
Received 14 May 2013
Received in revised form 11 September 2013
Accepted 26 September 2013
Available online xxxx

Editor: Pavlos Kassomenos

Keywords:
Europe
AOD
North–south gradient
Ozone
Aerosols
Emission distributions

ABSTRACT

Major gaseous and particulate pollutant levels over Europe in 2008 have been simulated using the offline-coupled WRFCMAQ chemistry and transport modeling system. The simulations are compared with surface observations from the EMEP stations, ozone (O_3) soundings, ship-borne O_3 and nitrogen dioxide (NO_2) observations in the western Mediterranean, tropospheric NO_2 vertical column densities from the SCIAMACHY instrument, and aerosol optical depths (AOD) from the AERONET. The results show that on average, surface O_3 levels are underestimated by 4 to 7% over the northern European EMEP stations while they are overestimated by 7–10% over the southern European EMEP stations and underestimated in the tropospheric column (by 10–20%). Particulate matter (PM) mass concentrations are underestimated by up to 60%, particularly in southern and eastern Europe, suggesting underestimated PM sources. Larger differences are calculated for individual aerosol components, particularly for organic and elemental carbon than for the total PM mass, indicating uncertainty in the combustion sources. Better agreement has been obtained for aerosol species over urban areas of the eastern Mediterranean, particularly for nss-SO_4^{2-}, attributed to the implementation of higher quality emission inventories for that area. Simulated AOD levels are lower than the AERONET observations by 10% on average, with average underestimations of 3% north of 40°N, attributed to the low anthropogenic emissions in the model and 22% south of 40°N, suggesting underestimated natural and resuspended dust emissions. Overall, the results reveal differences in the model performance between northern and southern Europe, suggesting significant differences in the representation of both anthropogenic and natural emissions in these regions. Budget analyses indicate that O_3 and peroxyacetyl nitrate (PAN) are transported from the free troposphere (FT) to the planetary boundary layer over Europe, while other species follow the reverse path and are then advected away from the source region.

1. Introduction

Air pollution can have significant impacts on ecosystems, human health, visibility and climate. Ozone (O_3) threatens human health (WMO, 2003) and vegetation (Fowler et al., 2009) and is an important greenhouse gas (IPCC, 2007). Fine and coarse particulate matter

* Corresponding author.
E-mail address: mariak@chemistry.uoc.gr (M. Kanakidou).
[1] Now at: Air and Climate Unit, Joint Research Centre, Ispra, Italy.

0048-9697/$ – see front matter © 2013 Elsevier B.V. All rights reserved.
http://dx.doi.org/10.1016/j.scitotenv.2013.09.090

(PM) have adverse impacts on human health (Becker et al., 2003; Nel, 2005). They also scatter and absorb the radiation in the atmosphere and alter cloud properties (Ramanathan et al., 2001) influencing the climate at local to regional scales. The European Commission has taken measures in order to decrease the concentrations of air pollutants such as O_3 (EC, 2002), nitrogen dioxide (NO_2) and sulfur dioxide (SO_2; European Commission, 2001), PM_{10} and $PsM_{2.5}$ (PM with aerodynamic diameter less than 10 μm and 2.5 μm, respectively; European Commission, 2008).

Over Europe, long term observations show different trends for different pollutants. Colette et al. (2011) investigated the air quality changes over Europe between 1998 and 2007, mainly focusing on O_3, NO_2 and PM_{10}, using data from the European Monitoring and Evaluation Programme (EMEP; www.emep.int) and the European Environmental Agency AIRBASE (http://acm.eionet.europa.eu/databases/AIRBASE/) networks. They reported a slight increase in O_3 levels, particularly in urban areas, that was attributed to the robust decrease of NO_2 throughout Europe. The decrease in NO_2 levels was not sufficient to depress the O_3 levels, mainly because volatile organic compound (VOC) emissions did not change much. Significant decreases of PM_{10} levels were found over western Europe and increases in southern Europe (Colette et al., 2011). In agreement with these results, Wilson et al. (2012) found positive annual trends of rural O_3 in central and north-western Europe and significant negative trends in eastern and south-western parts of Europe between 1996 and 2005. Through the use of satellite products, Vrekoussis et al. (2013) showed the decrease in tropospheric NO_2 levels over Greece following the reduction in emissions, particularly from 2008 and onward, due to the economic crisis.

Chemistry and transport models enable analysis of atmospheric composition changes and understanding of relations and feedbacks between meteorology, emissions and chemistry. For Europe, several studies focused on investigating the present and future levels of air quality indicators (Kukkonen et al., 2012 and references therein). The evaluation of the performances of these models through comparisons with observations is essential to increase confidence in the projected changes (Russell and Dennis, 2000). In this respect, Matthias (2008) found 30–60% underestimation of surface PM_{10} levels, comparably better agreement for the chemical composition (15–20% underestimation) and satisfactory simulations of the aerosol optical depth (AOD) levels over Europe for the years 2000 and 2001. Depending on season and location, Zyrichidou et al. (2009) found model over- and underestimations of the tropospheric NO_2 columns retrieved from Global Ozone Monitoring Experiment (GOME)/European Remote Sensing (ERS2), SCanning Imaging Absorption spectroMeter for Atmospheric CHartograpHY (SCIAMACHY)/Environmental Satellite (Envisat), Ozone Monitoring Instrument (OMI)/AURA and GOME-2/Meteorological Operational (MetOp) satellite observations over south-east Europe for the period 1996–2001, which were attributed to the uncertainties in emissions. Pay et al. (2010) have shown that the high resolution CALIOPE–EU model system was able to successfully simulate surface O_3 and NO_2 levels with a mean normalized bias (*MNB*) of 6% and −17%, respectively, and reproduced most of the PM pollutant events ($r = 0.5$–0.6) with underestimations ($MNB = -50\%$ and −45% for PM_{10} and $PM_{2.5}$, respectively) for the year 2004. Appel et al. (2012) evaluated the U.S. EPA Community Multiscale Air Quality (CMAQ) model performance over North America and Europe for the year 2006. They found daytime O_3 levels overestimated (by ~8%) in winter and by ~2% in summer and year-long underestimations of PM_{10} and $PM_{2.5}$ levels over Europe by ~25 to 65%. Basart et al. (2012) used the high resolution (12 km × 12 km) CALIOPE air quality modeling system to evaluate the daily-to-seasonal aerosol variability over Europe for the year 2004. They found that PM_{10}, $PM_{2.5}$ and AOD levels were underestimated due to underestimations in the fine fraction of carbonaceous matter (organic and elemental carbon) and secondary inorganic aerosols (SIA). They showed that PM_{10} north of 40°N was dominated by SIA while south of 40°N high PM levels were associated with desert dust. In general, differences between observations and models were mainly attributed to uncertainties in emissions, and to a lesser extent, to boundary conditions and spatial resolutions of the models.

The air pollution levels over Europe are likely to increase in a changing climate (Katragkou et al., 2011; Im et al., 2011, 2012; Megaritis et al., 2013). Among these studies, Katragkou et al. (2011) performed simulations using the Regional Climate Model (RegCM) v.3 and Comprehensive Air Quality Model with extensions (CAMx), which showed increases in surface O_3 particularly over southern Europe and the Mediterranean basin by up to 6 ppbv from 2041–2050 to 2091–2100. Im et al. (2011) calculated a 1 ppb yr^{-1} increase in surface O_3 levels over the eastern Mediterranean using the Weather Research and Forecasting mesoscale meteorological model (WRF)–CMAQ modeling system when increasing air temperatures homogeneously from +1 to +5 K. Megaritis et al. (2013) increased the temperatures uniformly by 2.5 and 5 K using PMCAMx-2008 chemistry and transport model and found increases in sulfate and organic aerosols (OA) in southern Europe and decreases in ammonium nitrate levels, particularly in central Europe. Similar results have been reported by Im et al. (2012) with increases in OA levels in south-eastern Europe due to increases in temperatures but decreases in sulfate levels due to significant reductions in-cloud-production of sulfate.

In this manuscript, air quality levels over the European domain (Fig. 1) for the entire year of 2008 have been investigated using the WRF–CMAQ model system in the frame of the EU-funded projects: Megacity-Zoom for the Environment (CityZen; https://wiki.met.no/cityzen/start) and Evaluating the Climate and Air Quality Impacts of Short-lived Pollutants (ECLIPSE; http://eclipse.nilu.no). The model performance in simulating air quality levels has been evaluated via comparisons with surface and satellite observations, as well as O_3 soundings. The budgets of major gaseous and particulate pollutants over Europe are calculated for the first time using a mesoscale chemistry and transport model (WRF–CMAQ) on a relatively high spatial and temporal resolution compared to the previous studies that employed global chemistry models (Aan de Brugh et al., 2011; Pozzer et al., 2012).

2. Materials and methods

2.1. Model system

The WRF–ARW (v3.1.1; Skamarock and Klemp, 2008) has been offline-coupled with the CMAQ model, v4.7 (Byun and Schere, 2006; Foley et al., 2010). The simulation period covers the year 2008 (366 days), which was one of the focus years of the CityZen project, with a spin-up period of 20 days from December 2007. The model domain (Fig. 1) covers most of Europe, North Africa and the Middle East (from 18.98°N, 3.58°W to 49.82°N, 57.64°E) on a 30 km horizontal resolution, extending up to 16 km height on 23 vertical levels. The physical and chemical model configurations are provided in detail by Im and Kanakidou (2012). Monthly initial and boundary conditions for the CMAQ model have been extracted from the global chemistry-transport model TM4-ECPL (Myriokefalitakis et al., 2011) on a 3° × 2° spatial resolution and 34 vertical levels up to 0.1 hPa (~60 km).

2.2. Emissions

European anthropogenic emissions are provided from the emission inventory of the French National Institute of Industrial Environment and Risks (INERIS: https://wiki.met.no/cityzen/page2/emissions) on a 10 km × 10 km spatial resolution, which is a re-gridded product of the 50 km × 50 km EMEP inventory (http://www.ceip.at/) covering Europe. Details on the European anthropogenic emissions and chemical and temporal disaggregation of the emissions can be found in Im and Kanakidou (2012). The emissions from the remaining areas (i.e. North Africa and the Middle East) have been provided by the CIRCE global emission inventory on a 0.1° × 0.1° spatial resolution (Pozzer et al., 2012). The non-methane volatile organic compound (NMVOC) emissions are speciated

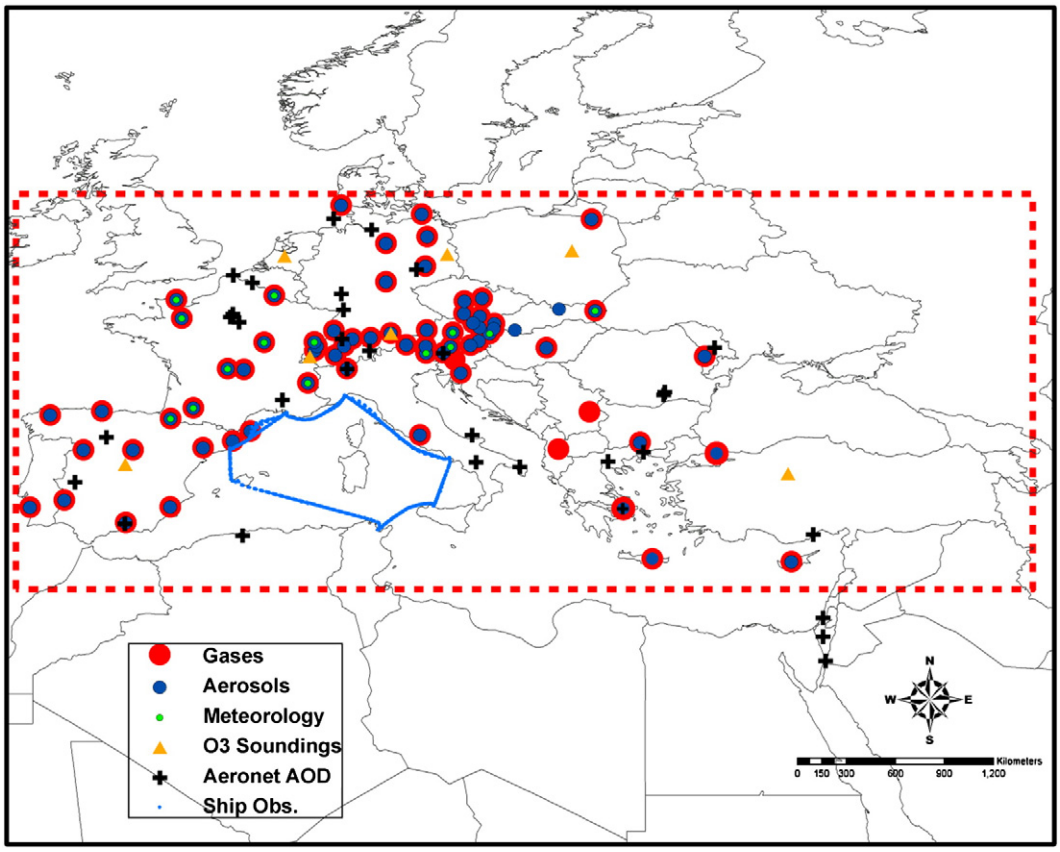

Fig. 1. Model domain (from 18.98°N, 3.58°W to 49.82°N, 57.64°E) and the locations of the EMEP (circles), WOUDC (triangles) and AERONET (crosses) monitoring stations as well as the ship routes (line) (June 26th to October 19th, 2008) used for the model evaluation. The inner frame shows the European region (from 26.91°N, 6.29°W to 51.04°N, 53.71°E) used for the budget calculations.

into 23 species using mean profiles from the EDGAR global inventory (Olivier et al., 2001) and the PM emissions are speciated into organic (OC) and elemental (EC) carbon, sulfates, nitrates and other species based on California Air Resources Board (CARB, 2007) profiles. The NMVOC emissions are then converted to CB05 species using the factors provided by Yardwood et al. (2005). The vertical distribution of emissions is calculated based on the Selected Nomenclature for Air Pollution (SNAP) codes provided by Simpson et al. (2003). Biogenic emissions are calculated online by the Model of Emissions of Gases and Aerosols from Nature (MEGAN; Guenther et al., 2006) module of the WRF–CHEM 3.1.1 (Grell et al., 2005). Wind-blown dust from African deserts (Sahara) can contribute between 10 and 70% to the PM_{10} levels in the Mediterranean region (Mitsakou et al., 2008; Theodosi et al., 2011). The natural dust emissions from the Sahara segregated in 5 aerosol sizes (0.2–2 μm, 2–4 μm, 4–6 μm, 6–12 μm, 12–18 μm) are calculated online by the GOCART (Georgia Tech/Goddard Global Ozone Chemistry Aerosol Radiation and Transport) dust module (Ginoux et al., 2001) of the WRF–CHEM model. The 5 size bins are mapped into the unspecified components of $PM_{2.5}$ and PM_{coarse} emissions following Tang et al. (2008; Eqs. (1) and (2)). The open-ocean and surf-zone sea-salt emissions are computed online by the CMAQ model. Open-ocean emissions are based on wind speed at 10 m (Gong, 2003) and linearly scaled based on the fraction of ocean area that is covered by whitecaps (Kelly et al., 2010). The biomass burning emissions have been calculated by the Fire Inventory from NCAR (FINN v.1) module of the WRF–CHEM model (Wiedinmyer et al., 2011). The FINN model provides daily open-fire emissions on a spatial resolution of 1 km, including wildfires, agricultural fires and prescribed burning using satellite observations of active fires and land cover, together with emission factors and estimated fuel loadings. The biomass burning emissions are distributed vertically using the profiles provided by Dentener et al. (2006).

$$PM_{2.5} = \text{bin1} + 0.4187 * \text{bin2} \quad (1)$$

$$PM_{coarse} = 0.5813 * \text{bin2} + \text{bin3} + 0.7685 * \text{bin4}. \quad (2)$$

The annually-integrated emissions from anthropogenic, biogenic, natural dust and biomass burning sources used in the model are presented in Table 1. Anthropogenic sources are the major contributors to the gaseous pollutants in the region, whereas for PM_{10}, natural dust emissions are 2 orders of magnitude higher than anthropogenic PM_{10} emissions. The here-calculated North African dust emissions (400 Tg yr^{-1}) are within the range of literature estimates (170–1430 Tg yr^{-1}, Engelstaedter et al. (2006) and 400–2200 Tg yr^{-1}, Huneeus et al. (2011)), considering that our domain does not cover the entire north Africa. In addition, the annual VOC emissions from biomass burning are estimated to be twice the biogenic VOC emissions; they are, however, more than 2 orders of magnitude lower than the anthropogenic VOC emissions. The spatial distributions of annually-integrated NO and $PM_{2.5}$ emissions are depicted in Fig. S1. Hot spot emission regions of London, Paris, Benelux, Po Valley, Istanbul and Cairo are clearly seen in that figure.

2.3. Observations

Available surface observations of concentrations of gaseous and particulate pollutants from the EMEP network for the whole simulation domain are taken from the EBAS project system (http://ebas.nilu.no/; Fig. 1, Tables S1 and S2 for the stations measuring gaseous and particulate

Table 1
Annual domain-integrated emissions used in CMAQ. Units are in Gg yr^{-1}.

	CO	NO_x	SO_2	NH_3	VOC	PM_{10}
Anthropogenic	4.3E + 04	1.7E + 04	1.4E + 04	5.7E + 3	2.1E + 04	3.5E + 03
Biogenic	1.4E − 01	6.8E + 02			6.3E + 04[a]	
Dust						3.6E + 05[b]
Biomass burning	4.4E + 01	2.2E + 00	1.9E − 01	8.7E − 01	3.3E + 01[c]	1.8E + 00[d]

[a] Biogenic VOCs are the sum of isoprene, monoterpenes, sesquiterpenes and other NMVOCs.
[b] Dust emissions are the sum of fine and coarse natural dust emissions.
[c] Biomass burning VOCs emissions are the sum of isoprene and other NMVOCs.
[d] Biomass burning PM_{10} emissions here applied are the sum of OC and BC.

species, respectively). In EMEP, stations are classified as rural background (RB) or remote (G). For simplicity, stations located higher than 1000 m are further classified as 'Free Troposphere' (FT) in the present study, although PBL height varies significantly and can exceed 1000 m, particularly during summer. Additional surface observations of gaseous and particulate pollutants for the eastern Mediterranean area on a higher spatial resolution covering Istanbul (IST), Athens (ATH1 and ATH2; classification based on the location within a particular grid cell) and Finokalia (FKL: Crete) have been provided in the frame of the CityZen project (see Table S3 for the station groups). Observations from the urban sites in Istanbul and Athens have been provided by the Air Quality Network of Istanbul Metropolitan Municipality (www.havaizleme.gov.tr) and the Hellenic Ministry of Environment Energy and Climate Change (http://www.ypeka.gr). PM_{10} and its chemical composition from a suburban site in Istanbul (ESC) for 2008 (Theodosi et al., 2010), surface O_3 mixing ratios in a semi-rural site in Istanbul (Im et al., 2013), $PM_{2.5}$ and its chemical composition in Athens (Paraskevopoulou et al., 2012; Pateraki et al., 2012), and PM_{10}, $PM_{2.5}$ and chemical composition data from Finokalia (FKL: http://finokalia.chemistry.uoc.gr; Mihalopoulos N. and coworkers unpublished data) are also used in the present study.

Ship-borne O_3 and NO_x observations in the western Mediterranean from June 26th to October 19th, 2008 are used to evaluate the model performance over the sea. These ship-borne measurements were carried out automatically by analyzers placed on the cruise ship 'Costa Magica' by the Joint Research Centre of the European Commission. The ship followed a fixed weekly route in the western Mediterranean (Fig. 1) during the studied period. The observations have been provided as 10-minute averages and hourly mean values are calculated to be compared with CMAQ values in each grid cell along the ship tracks. Risk of contamination from the stack of the ship has been eliminated based on the relative wind that has been recorded: conditions where the relative wind comes behind the ship within ±40° have been removed from the dataset. A detailed description of this measurement facility is given by Schembari et al. (2012). Observed vertical ozone profiles (ozone soundings) from the World Ozone and Ultraviolet Radiation Data Center (WOUDC; http://www.woudc.org/) for 7 stations over Europe where data are available for the studied period and domain have been also used (Table S4). Fig. 1 shows the locations of all monitoring stations used for the model evaluation.

The tropospheric NO_2 vertical column densities (VCDs) retrieved from SCIAMACHY (Burrows et al., 1995) satellite observations are compared to the simulated NO_2 tropospheric columns. SCIAMACHY was located on-board the ENVISAT that operated from March 2002 to April 2012 and provided VCDs of NO_2 on a 60 × 30 km spatial resolution (Richter et al., 2005). SCIAMACHY NO_2 observations have been validated by Heue et al. (2005) for southern Europe. The SCIAMACHY data derived on a 0.5° × 0.5° spatial resolution are interpolated on the CMAQ output that is on a 30 km spatial resolution. The four corners of each SCIAMACHY grid cell have been located on the projection of the CMAQ domain and the SCIAMACHY grid is intersected with the neighboring CMAQ grids at corresponding time of SCIAMACHY measurements (10:00 LST) as explained in Shi et al. (2008). The SCIAMACHY and CMAQ products are compared on a grid basis.

Daily-averaged Aerosol Optical Depths (AOD) from the 33 Aerosol Robotic Network (AERONET; http://aeronet.gsfc.nasa.gov/new_web/index.html) stations (Table S5) have also been used for model evaluation.

2.4. Model derived AOD

AOD is calculated using reconstructed extinction that depends on aerosol mass and humidity (Eq. (3); Malm et al., 1994). This approach has been widely used to compare AOD from CMAQ with observations (Roy et al., 2007; Matthias, 2008). The Malm et al. (1994) approach is suitable for the mid-visible spectrum around wavelengths of 500 nm and therefore, AOD observations at 500 nm from the level 2 (cloud-cleared and quality-assured) are used for model validations.

$$\alpha_{ext} = 0.003\, f(RH)(m_{NH4} + m_{NO3} + m_{SO4}) + 0.004 m_{OM} + 0.01 m_{EC} + 0.001 m_{PM2.5_{oth}} + 0.0006 m_{PM_{coarse}} \quad (3)$$

where m denotes the mass concentration of the given aerosol components in mg m^{-3} and $f(RH)$ denotes the light scattering relative humidity adjustment factor from the lookup table provided by the Interagency Monitoring of PRotected Visual Environments (IMPROVE) database (http://vista.cira.colostate.edu/improve/Tools/humidity_correction.htm). The specific scattering coefficients (0.003, 0.004, 0.001 and 0.0006) have units of m^2 mg^{-1} and are based on the assumption of a log-normal particle size distribution (Malm et al., 1994). OM denotes for organic matter, $PM_{2.5other}$ denotes fine unspecified aerosols and PM_{coarse} denotes coarse aerosols (sea-salt, dust, coarse inorganics and unspecified coarse material).

The model performance has been evaluated by comparing the simulated pollutant levels with surface and vertical observations using a number of statistical parameters. The statistical parameters used in the present study are correlation coefficient (r), *BIAS*, normalized mean bias (*NMB*), root mean square error (*RMSE*), mean absolute gross error (*MAGE*), normalized mean error (*NME*) and index of agreement (*IOA*). The definitions of these parameters are provided in the Supplementary material. Observations at stations that fall into the same model grid (as is the case for Istanbul and Athens observations) have been averaged and then compared with the model results.

2.5. Budget analysis

Integrated pollutant fluxes by advection (ADV2: sum of advection in x and y directions), convection (ZADV), emissions (EMIS), dry deposition (DDEP), chemistry (CHEM), aerosol processes (AERO: particle formation, condensation, coagulation and aerosol thermodynamics) and cloud processes (CLDS: aqueous chemistry, below- and in-cloud mixing, cloud scavenging, and wet deposition) are calculated for O_3, NO_x, peroxyacetyl nitrate (PAN), nitric acid (HNO_3), SO_2, non seasalt-sulfate (nss-SO_4^{2-}), nitrate aerosol (NO_3^-), ammonium aerosol (NH_4^+), particulate organic carbon (OC), elemental carbon (EC) and PM_{10} over Europe (Fig. 1; inner frame) on an annual basis using the Integrated Process Analysis (IPR) tool of the CMAQ model. The calculations are done

for the surface layer, within the planetary boundary layer (PBL) that corresponds to the lowest 11 model layers, and within the free troposphere (FT), which is defined as all the layers above the PBL. Hourly PBL heights are calculated by the Meteorology–Chemistry Interface Processor (MCIP: Otte and Pleim, 2010) and the budget terms at the corresponding layers for each hour have been extracted from the IPR outputs and integrated over the PBL height.

3. Results

3.1. Comparison of CMAQ simulations with observations

3.1.1. Gaseous pollutants

Simulated surface mixing ratios of O_3, NO_2, CO and SO_2 are compared with hourly O_3 and daily NO_2, CO and SO_2 observations and the model performance statistics are given in Table 2 for O_3 and NO_2 and Table S6 for CO and SO_2. The point-by-point comparisons (scatter plots) for O_3 at the EMEP stations (RB and FT), Istanbul and Athens urban station groups are depicted in Fig. S2. Temporal variations of O_3 mixing ratios are well captured by the model at the EMEP sites ($r > 0.6$) while annual mean mixing ratios are overestimated by ~2% at the EMEP RB sites and underestimated at the FT sites by ~16% (Table 2). NO_2 shows a large overestimation at the FT sites ($NMB = 87\%$). An outlook of the model performance at the northwestern (NW), northeastern (NE), southwestern (SW) and southeastern (SE) European stations for the major gas and aerosol species is provided in Fig. 2. Although there is no spatial pattern in the biases on a station-by-station basis for the EMEP stations within the domain, on average, surface O_3 mixing ratios are underestimated by 7% and 4% over the NW and NE Europe, respectively, and overestimated by 7% and 10% over the SW and SE Europe, respectively (Fig. 2a). These results are in agreement with the Monitoring Atmospheric Composition and Climate (MACC) reanalysis (Inness et al., 2013). The temporal variation of O_3 mixing ratios at the eastern Mediterranean urban sites is better simulated ($r \geq 0.8$) than elsewhere over Europe most possibly due to the updated emission inventory for the eastern Mediterranean. Markakis et al. (2010 and 2012) reported differences varying between ~10% to a factor of 4 differences in O_3 precursor emissions of EMEP inventory and the new inventories for Greece and Istanbul used in the present study. In Greece O_3 levels are overestimated by ~4–17% with errors in the range of 20–30% (Table 2). The larger overestimation at the FKL remote downwind station (NMB ~17%) compared to the ATH1 and ATH2 stations (NMB ~3–4%) suggests overestimations in the transport of O_3 precursors to the site, and in O_3 photochemical production and underestimation in dry deposition of O_3 that is attributed to the high water fraction of the corresponding model grid cell. On the opposite, O_3 levels in Istanbul are underestimated by less than 1% (Table 2 and Fig. S2c), however with a large error of ~30% (Table 2). Particularly the relatively coarse resolution of the model can artificially dilute the NO_x emissions leading to reduced NO_x-titration and thus, overestimation of the O_3 levels in the urban areas (Im and Kanakidou, 2012).

Hourly ship-borne measurements of O_3 and OX ($O_3 + NO_2$) from June to October 2008 and the corresponding CMAQ results are depicted in Fig. 3 distinguishing those over the sea from those in the harbors. As seen in this figure, the variability of both O_3 and OX is captured slightly better in the harbors ($r = 0.6$; Number of pairs (N) = 556) compared to the open sea ($r = 0.5$; N = 1060), while the computed O_3 levels in the harbors show larger overestimation of the observations ($NMB = 39\%$) than over the sea ($NMB = 22\%$). This can be attributed to better representation of the seasonality of precursor emissions over the harbors compared to the open sea. On the other hand, this is possibly due to the underestimation of emissions in the harbors where O_3 is titrated by high concentrations of NO. On a monthly basis, NO_x is underestimated in all months by 10% to 50% while O_3 is overestimated by 18 to 35% in all studied months. These deviations of NO_x simulations from the observations may also be attributed to potential positive artifacts of NO_2 measurements due to the presence of PAN and HNO_3 that may also be converted to NO. The simulated O_3 seasonality is in general agreement with that observed, with O_3 levels decreasing from June to September.

The comparisons of WOUDC ozone sounding data with model results show that O_3 levels are generally underestimated by 10–20% from surface to around 850–900 hPa (Fig. 4), except for the stn316

Table 2
Statistical comparison of the observed and simulated daily surface concentrations of O_3, NO_2, PM_{10}, $PM_{2.5}$, NO_2 VCDs and AODs. *N* denotes the number of pairs for comparisons, *NMB* and *NME* are in %, *R* and *IOA* are unitless, *BIAS*, *RMSE* and *MAGE* are in units of ppb for surface O_3 and NO_2, μg m^{-3} for PM_{10} and $PM_{2.5}$, molecules cm^{-2} for NO_2 VCDs and unitless for AODs. RB denotes Remote Background and FT stands for Free Troposphere.

	Stations	N	R	BIAS	NMB	RMSE	MAGE	NME	IOA
O_3	RB	13,226	0.7	0.5	1.6	9.6	0.2	71.9	0.8
	FT	5405	0.6	−6.7	−16.3	12.1	1.0	2.3	0.7
	ATH1	365	0.8	9.1	4.4	15.3	11.6	33.7	0.8
	ATH2	366	0.8	1.0	3.4	9.4	7.1	22.0	0.9
	FKL	281	0.8	8.0	17.4	10.8	9.0	19.7	0.8
	IST	366	0.9	−0.4	−0.5	9.1	7.4	33.9	0.9
NO_2	RB	7951	0.7	0.1	5.3	2.2	1.4	54.2	0.8
	FT	2287	0.4	1.0	87.0	2.5	1.5	126.9	0.5
	ATH1	8784	0.3	−21.6	−41.7	31.2	25.8	50.0	0.5
	ATH2	5658	0.2	−3.3	−9.3	35.7	25.3	72.2	0.5
	IST1	3054	0.4	0.1	0.3	50.2	31.8	60.1	0.6
	IST2	8783	0.1	5.7	6.4	80.4	56.3	62.8	0.4
PM_{10}	RB	9162	0.4	−4.1	−24.0	14.9	0.8	4.6	0.6
	FT	2202	0.4	−0.8	−7.4	11.8	1.4	14.7	0.6
	ATH1	366	0.8	−10.0	−29.7	14.7	13.5	38.8	0.8
	ATH2	366	0.7	−12.8	−38.4	18.0	17.9	41.6	0.7
	FKL	215	0.6	3.2	14.2	13.6	8.0	40.2	0.7
	IST1	284	0.7	−27.4	−47.2	35.4	27.9	47.9	0.7
	IST2	366	0.7	−19.6	−32.9	26.9	22.0	36.9	0.7
	ESC	143	0.6	−10.2	−22.5	23.0	14.9	37.6	0.7
$PM_{2.5}$	RB	5998	0.3	−4.3	−36.1	11.9	0.6	4.8	0.5
	FT	1291	0.2	−0.4	−5.7	7.9	2.1	29.9	0.5
	ATH1	70	0.3	−13.2	−53.4	16.3	14.5	58.7	0.5
	ATH2	108	0.3	−10.4	−45.4	14.6	12.4	54.1	0.5
NO_2 VCDs	Domain	19,394	0.9	5.6E + 14	38.1	1.2E + 15	7.7E + 14	52.4	0.9
AOD	AERONET	5028	0.5	>−0.1	−10.5	0.2	0.1	49.1	0.7

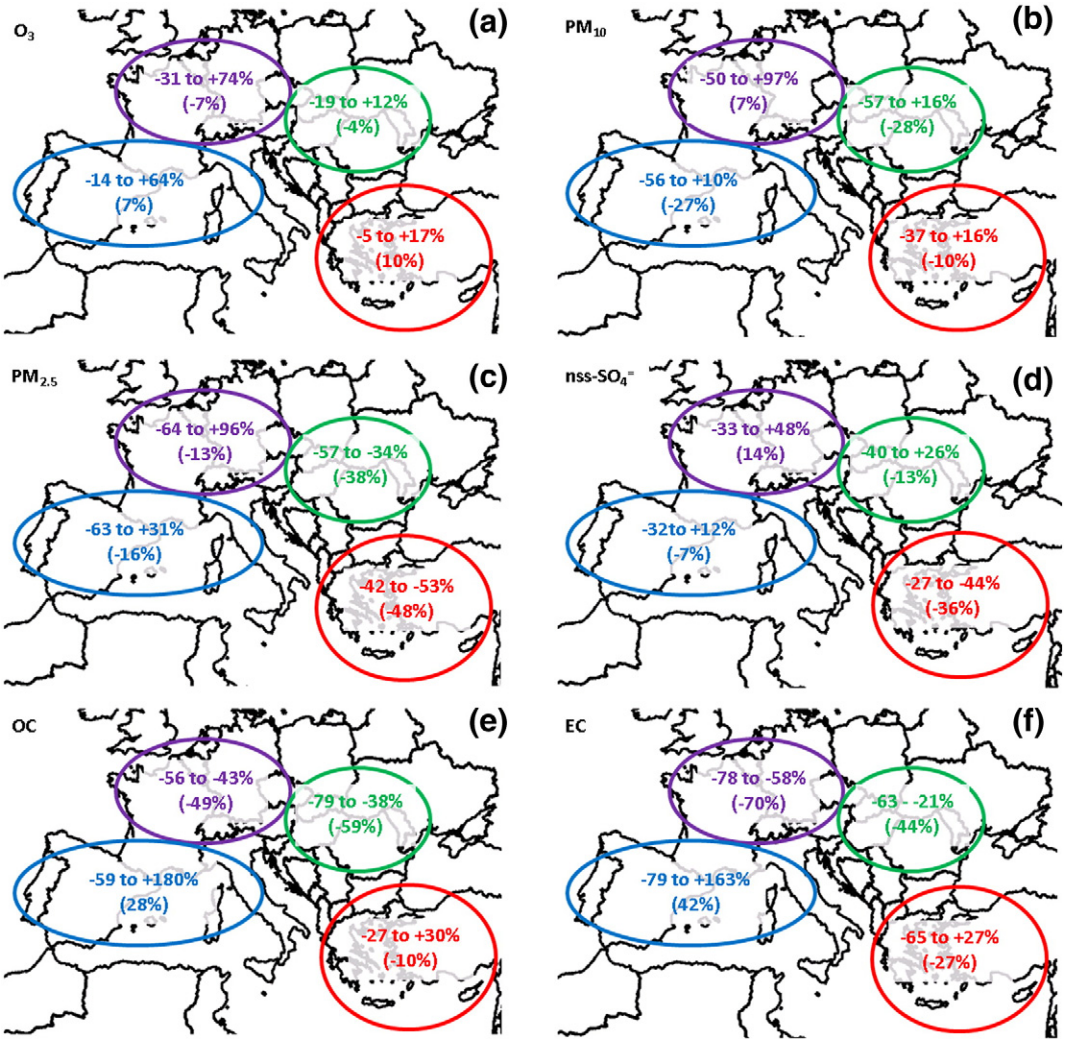

Fig. 2. Model performance spatially-classified based on the normalized mean bias (*NMB*) calculated on a daily basis for (a) O_3, (b) PM_{10}, (c) $PM_{2.5}$, (d) nss-SO_4^{2-}, (e) OC and (f) EC. The ranges show the minimum and maximum computed *NMB* values for the individual stations within each area, while the parentheses show the mean *NMB* for the particular station group (individual station locations are given in Tables S2 and S3).

station (De Bilt, the Netherlands). The model performance is very poor at this station, most likely due to its proximity to the northern boundary of the model domain that leads to additional uncertainties due to the boundary conditions. For the other stations, r values are ~0.7–0.8, with O_3 underestimations of 10–20% and MAGE of 30–50% (Table S7). These results show that the model reasonably simulates the O_3 profiles in the lower and mid troposphere, while it performs moderately in the upper troposphere, indicating limitations of the model to represent the stratosphere–troposphere exchanges of O_3 as well as uncertainties originating from the boundary conditions provided by the global model.

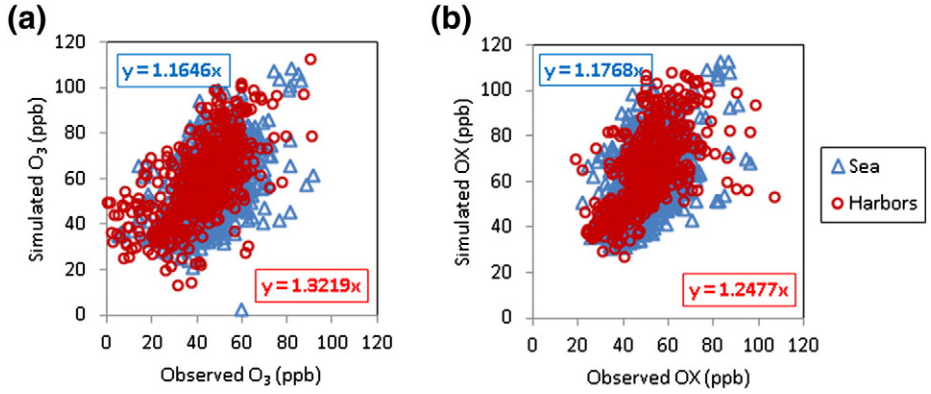

Fig. 3. Scatter plots of hourly ship-borne and simulated O_3 (a) and OX (b) levels in the western Mediterranean (see Fig. 1 for the ship tracks). Red circles show the levels in the harbors while blue triangles show the levels only over the sea. (For interpretation of the references to color in this figure legend, the reader is referred to the web version of this article.)

The model performance in simulating the temporal variations of simulated surface NO_2 mixing ratios vary largely between the station groups ($r = 0.1$–0.7). *NMB* values are generally low (up to 5% at surface) except for the ATH1 station group (*NMB* = ~42%), while *NME* values above 50% are calculated for all station groups (Table 2). CO levels at the EMEP stations are underestimated by ~10–15% while larger underestimations are computed for the ATH (75%) and IST (35%) station groups (Table S6) that may be attributed to the limited representation of the urban emissions in a relatively coarse resolution model. SO_2 levels are overestimated at all stations, particularly at the EMEP RB stations (almost by a factor of 2). The errors in the simulated precursors also introduce errors in the calculated production of secondary gases and aerosols. For instance, at rural locations, overestimations in CO and NO_2 may lead to overestimations in O_3 production, while overestimated SO_2 levels may also imply underestimated sulfate aerosol formation in addition to overestimated SO_2 emissions, as will be further discussed.

3.1.2. Particulate matter

Comparisons of simulated surface PM_{10} and $PM_{2.5}$ mass concentrations with observations are presented in Table 2. PM_{10} levels are moderately simulated at the EMEP sites (Fig. S3a). Temporal variation at the remote station of Finokalia is better captured ($r = 0.6$) compared to RB and FT stations ($r = 0.4$). Acceptable underestimations (*NMB* = ~10–20%) are calculated for the EMEP stations. The model generally underestimates the PM_{10} levels at the EMEP stations with relatively better performance over SE Europe (Fig. 2b). This might be partially due to the model parameterizations that does not allow particles to settle from higher to lower layers and thus to the surface layer. Underestimations larger than 50% are computed over the NE and SW Europe, while over NW Europe there are large overestimations at some stations over Germany resulting in an overestimation in the region. At the urban station groups in the eastern Mediterranean (in Istanbul and Athens), temporal PM_{10} variations are better represented by the model ($r = 0.7$–0.8) than at the EMEP stations ($r = 0.4$–0.6). However, urban PM_{10} levels are largely underestimated (*NMB* = −30% to −50%; Table 2, Fig. S3b and c) compared to the suburban (ESC; *NMB* = −22%) and rural (FKL; *NMB* = 14%; Fig. S3d) levels. These findings suggest the potential underestimation of urban particulate emissions, as expected since those from resuspended dust are missing in the present study and can contribute up to 20–25% to PM_{10} levels in the Mediterranean region (Nicolas et al., 2008; Karanasiou et al., 2011; Koçak et al., 2011). $PM_{2.5}$ temporal variations are poorly simulated at all station groups ($r = 0.2$–0.3). Similar to the PM_{10} levels, computed $PM_{2.5}$ levels show larger underestimations at the urban station groups in the eastern Mediterranean (*NMB* = −45% to −55%) compared to EMEP stations (*NMB* = −5% to −35%; (Table 2). These results support the hypothesis that anthropogenic emissions are a key uncertainty for PM as $PM_{2.5}$ is largely anthropogenic in origin. The aerosol chemical composition, further discussed, provides some insight to the emission sectors mainly responsible for these discrepancies. A similar spatial performance pattern is observed for PM_{10}, with large overestimation over NW Europe (Fig. 2c).

3.1.3. Aerosol chemical composition

The simulated mass concentrations of nss-SO_4^{2-}, NO_3^-, NH_4^+, particulate organic carbon (OC) and elemental carbon (EC) are compared with observations for the different aerosol sizes where available (detailed results are presented in Table S8). As will be further discussed, there is a general underestimation of inorganic aerosols on annual and seasonal bases. These differences can be attributed to uncertainties in emissions and meteorology, as well as the spatial resolution of the model that can be considered relatively coarse for urban areas. Part of the discrepancies between the observed and simulated inorganic aerosol levels can also be attributed to the lack of consideration of crustal materials in the ISORROPIA v1.7 (Nenes et al., 1998) thermodynamic equilibrium model. These interactions between the inorganic and dust aerosol components are important particularly over southern Europe.

3.1.3.1. Secondary inorganic aerosols. The temporal variations of nss-SO_4^{2-} levels are reasonably captured by the model ($r = 0.4$ to 0.9) while the levels are underestimated by 10–45% in both PM fractions, with the highest underestimations calculated in the fine fraction (Table S8 and Fig. S4) except for the FT stations where they are overestimated by 28%. This can be due to an underestimate by the model of SO_2 oxidation and thus of $SO_4^=$ formation in the boundary layer, enabling more SO_2 to reach the FT and being oxidized there to $SO_4^=$. Similar to the total PM mass, nss-SO_4^{2-} levels are underestimated more at the urban than the rural and remote sites (Table S8). Beside potential emission inaccuracies, these underestimations may result from the insufficient gas-to-particle conversion of SO_2 to nss-SO_4^{2-} as indicated by the SO_2 levels that are overestimated by the model (Table S6). Indeed, neutralization of nss-SO_4^{2-} by NH_4^+ is underestimated. This is shown by the higher observed than modeled slope of correlation between NH_4^+ and nss-SO_4^{2-} equivalents (observed = 0.7–0.9; modeled = 0.5–0.8). The computed spatial distribution of nss-SO_4^{2-} levels is generally underestimated over all of

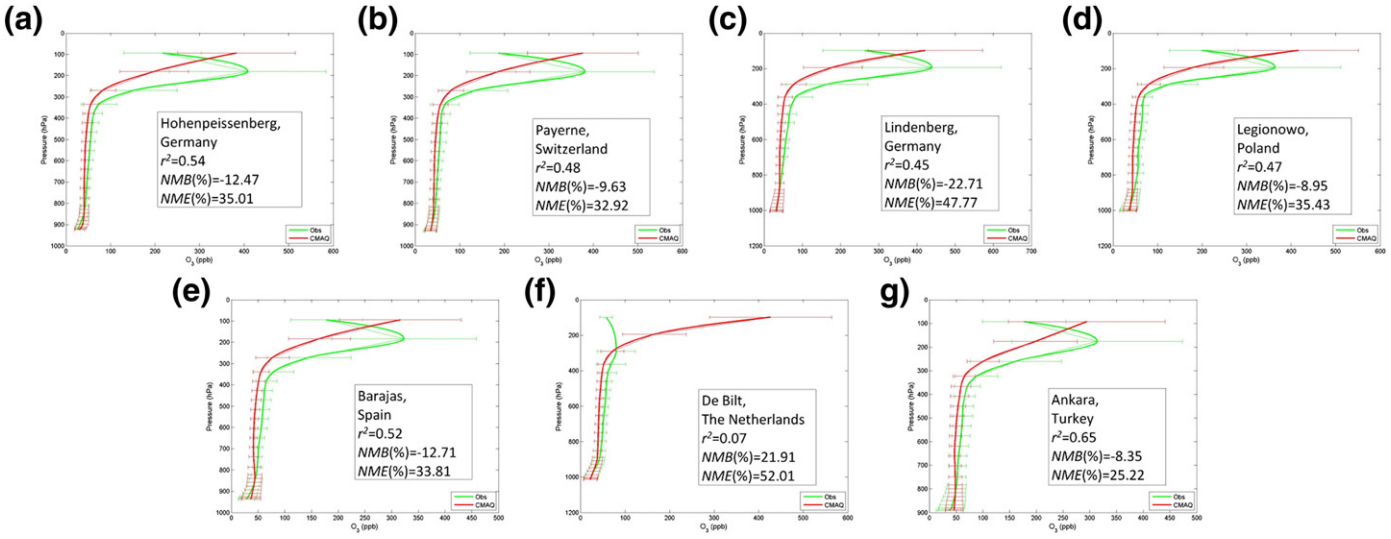

Fig. 4. Comparison of observed and simulated vertical ozone profiles over the WOUDC stations (Table S4).

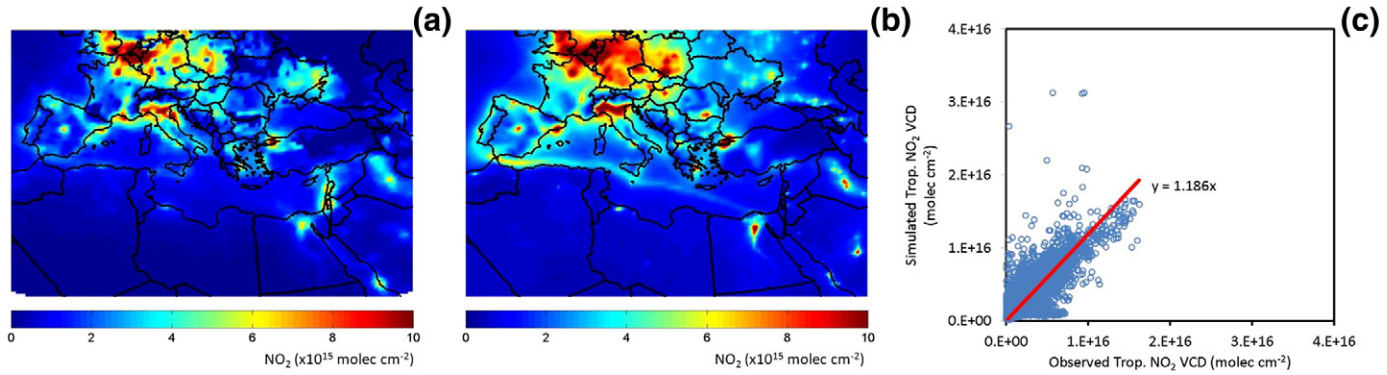

Fig. 5. SCIAMACHY-observed (a) and CMAQ-calculated (b) tropospheric NO_2 VCD distributions, averaged over the simulation period (entire 2008) and (c) scatter diagram of grid-based observed and simulated annual mean NO_2 VCDs.

Europe except for NW Europe, similar to the model performance for PM_{10} and $PM_{2.5}$, following the anthropogenic emissions (Fig. 2d) and their speciation profiles as discussed in Section 2.2. Opposite to nss-SO_4^{2-} levels, NO_3^- levels are generally overestimated from a few percent to a factor of three (Table S8). Overall, although significant discrepancies exist between observations and simulations, better agreement is achieved compared to earlier modeling studies for the eastern Mediterranean region (Im et al., 2012).

3.1.3.2. OC and EC. OC and EC levels are mostly underestimated by 30–60% (Fig. 2, Fig. S5 and S6), with larger differences at the urban sites (Table S8) in line with the fact that OC and EC levels are largely anthropogenically driven, particularly by fossil fuel or biomass combustion sources. OC levels in the PM_{10} fraction are underestimated by 36% while they are underestimated by 66% in the $PM_{2.5}$ fraction at the RB stations. This difference is partly due to the different stations measuring OC levels in different size fractions as well as the anthropogenic origin of the OC emissions. The overestimations are largely observed at the southern European stations (Fig. 2e and f). The poor-to-moderate correlations (r = ~0.4–0.6 for OC and r = ~0.1–0.6 for EC, Table S8) imply the uncertainties associated with the emissions since EC is a primary pollutant and OC also has a large primary component. Systematic OC and EC overestimations are calculated both in PM_{10} and $PM_{2.5}$ fractions at the stations in Spain, suggesting that anthropogenic emissions are possibly overestimated in Spain (Fig. 2e).

To investigate the model's capability to simulate the secondary organic aerosol (SOA) in the atmosphere, the OC/EC ratio has been analyzed. High OC/EC ratios indicate SOA formation. OC/EC ratios have been derived both from the observations and from the model results. For the FT stations, the observed OC/EC ratios in the PM_{10} and $PM_{2.5}$ fractions (12 and 21, respectively) are largely underestimated by the model (by a factor of ~5). Observed OC/EC ratios in the PM_{10} and $PM_{2.5}$ fractions at the EMEP RB sites and the urban sites in the eastern Mediterranean are also generally underestimated. In addition, computed EC levels are significantly lower than observations possibly due to underestimated anthropogenic emissions (Table S8) as found in earlier studies (Im and Kanakidou, 2012). These results indicate a large underestimation of the SOA. Similar results were found by Im et al. (2012) for the eastern Mediterranean and were attributed to the lack of long chain-alkane chemistry in the CB05 chemical mechanism (Carlton et al., 2010) that is used in the present study.

3.1.4. Model comparison with SCIAMACHY and AERONET observations

Simulated NO_2 VCDs at 1000 LT are compared with tropospheric column amounts of NO_2 derived from the SCIAMACHY observations (Fig. 5) and statistics of this comparison are provided in Table 2. Table S9 provides the seasonal comparisons of observed and simulated NO_2 VCDs and AODs. As seen in Fig. 5a and b, the spatial distribution of NO_2 VCDs is generally well captured by the model, although the absolute levels are overestimated. There are large overestimations, particularly over Germany and Poland. The shipping routes also clearly stand out in the simulated columns, while the observations do not show such high levels of NO_2. Although Istanbul, Athens and Cairo stand out as hot spots in the SCIAMACHY observations, the model calculates larger than observed NO_2 columns over these eastern Mediterranean cities (by a factor of ~2 over Istanbul and Cairo extended areas and ~18% over Athens extended area). In contrast, the model is not able to capture the hot spots over Lebanon and Israel. These differences can be attributed to potential underestimation of the emissions over these areas (see Fig. S1a) as has been found for Athens in Greece and for Istanbul in Turkey by Markakis et al. (2010, 2012). Table 2 also shows that the overall spatial distribution of NO_2 column is reasonably represented by the model (r = 0.9), while levels are overestimated by 38% compared to SCIAMACHY retrievals with a *NME* of 52%.

Depending on the satellite and the retrieval algorithm, Zyrichidou et al. (2009) found overestimations in rural regions and some industrial regions of south-east Europe, where the emissions and background conditions may have not been well represented in their model. The differences can be attributed to i) the larger spatial resolution of the satellite observations ($0.5° \times 0.5°$) and the model (30 km × 30 km), ii) uncertainties originating from the vertical resolution of the model, iii) the measurement errors due to the uncertainties from clouds, air mass factors, surface reflectivity and aerosols (Richter and Burrows, 2002), and iv) uncertainties in the emissions (Shi et al., 2008; Han et al., 2011) since most of the tropospheric NO_2 is located in the lower troposphere and thus strongly driven by emissions.

Model performance statistics for the comparison of simulated AOD values to observations at the 33 AERONET stations in the model domain (Table S5) are provided in Table 2, while the station-based statistics are presented in Table S10. Results show that the model generally underestimates the observed AOD values by ~2% to ~45% (with a mean underestimation of ~11%, Table 2) while the temporal distributions are reasonably simulated with r values ranging from ~0.3 to ~0.6. The differences (Table S10) reflect those in the simulated mass concentrations of the AOD-relevant aerosol components (Table S8). As seen in Table S10, observed AOD values at the AERONET stations north of 40°N are both overestimated and underestimated depending on location (e.g. by 1.2% (Lie, France) to 28.7% (Laegeren, Switzerland) or underestimated by −2.2% (Paris, France) to −35.1% (Tremiti, Italy). An average deviation from observations of −2.7% is calculated for these stations. On the other hand, the model only underestimates AOD by −3.9% (FORTH, Crete) to −44.4% (Nes Ziona, Israel) south of 40°N, with a mean underestimation of −22.1%. This larger deviation of model results from observations in southern than in northern Europe can be attributed to a large model underestimation of the abundance of dust in southern Europe, as will be discussed in Section 3.2. It should be noted that

AOD is not only related to the aerosol component mass, but also depends on the shape and size distribution of the particles (see assumption in Section 2.4). Differences can also be attributed to the relative humidity correction since uncertainties in the relative humidity calculations can lead to large deviations in the reconstructed AOD (Matthias, 2008).

3.2. Simulated spatial distribution of pollutants

The spatial distributions of annual mean surface O_3, NO_2, PM_{10}, nss-SO_4^{2-}, NO_3^-, NH_4^+, OC and EC are depicted in Fig. 6. There is a clear gradient in O_3 between the north and the south parts of the domain around 40°N (Fig. 6a) that can be attributed to higher temperatures and solar radiation and thus, more intense photochemistry over southern Europe and North Africa compared to northern Europe. Higher anthropogenic NO_x emissions in northern Europe also lead to stronger O_3-titration compared to the south. The NO_2 hot spot areas due to these emissions are clearly seen in the simulated surface NO_2 levels in Fig. 6b. The Benelux area, Paris, Po valley, Istanbul, Cairo and Athens are areas where high NO_2 levels are simulated. Particularly, the Mediterranean Sea experiences the highest O_3 levels due to the lower dry deposition of O_3 over water than land, the intensive regional photochemistry and the reception of upwind pollution. In addition, boundary layer heights tend to be lower over water, which may contribute to higher O_3 levels over water. However, there is a corridor of lower O_3 than the surrounding region that extends throughout the Mediterranean Sea due to the titration of O_3 by NO_x emissions from shipping. Fig. 6a also shows higher O_3 levels over the east Mediterranean than the western Mediterranean. Large urban agglomerations in the eastern Mediterranean (Istanbul, Cairo and Athens) also stand out with low O_3 levels due to high NO_x levels.

A similar south to north gradient is also seen for the surface PM_{10} levels (Fig. 6c). Southern Europe experiences higher PM_{10} levels than northern latitudes due to the Saharan dust contribution. Over the eastern Mediterranean, nss-SO_4^{2-} contributes significantly to the aerosol mass (Fig. 6d) while NO_3^- (Fig. 6e) and NH_4^+ (Fig. 6f) are simulated to be high over central and western Europe. NO_3^- levels are also high over the eastern Mediterranean Sea due to the existence of the sea-salt particles. These results are in agreement with Querol et al. (2009) that reported a north-to-south and east-to-west gradient of aerosol levels in the Mediterranean. The OC and EC distributions clearly show the urban emission hot spots as well as the shipping routes (Fig. 6g and h). Very high OC and EC levels are calculated over the urban areas of the eastern Mediterranean basin as well as over Benelux and Po Valley due to high anthropogenic emissions. In northern Europe (latitude>40°N), computed PM_{10} is dominated by SIA (41%) and carbonaceous matter (~14%) while dust and sea-salt comprise only 31% (10% and 21%, respectively) of PM_{10}. Conversely, in southern Europe (latitude < 40°N, excluding North Africa), SIA and carbonaceous matter comprise only 21% while dust and sea-salt contribute 43% (31% and 12%, respectively). These results are in agreement with previous findings reported by Basart et al. (2012). Simulated $PM_{2.5}/PM_{10}$ ratios are 0.6 and 0.5 in northern and southern Europe, respectively, suggesting higher anthropogenic contribution in northern Europe. Over both northern and southern Europe, CMAQ simulations indicate primary OA contribute more than 80% to the total OA, suggesting underestimated aerosol aging as discussed in Section 3.1.3.2.

3.3. Budget analysis

Annual budgets (see Section 2.5) of the major gaseous and particulate pollutants over Europe (Fig. 1; inner frame) are calculated with the CMAQ model at the surface and within the PBL and FT. The net budgets of these species over Europe are presented in Table 3.

Results show that advection (ADV2) is a net sink for most species over Europe on an annual basis in all atmospheric compartments (the surface layer alone but also within the entire PBL and the FT) indicating that Europe acts as a net source of most species for the surrounding region. While vertical transport (ZADV) is a net source at the surface for most species (except PM_{10}), it is a sink in the PBL except for PAN and O_3, suggesting vertical transport from the PBL to the surface or the upper troposphere depending on the pollutant (Table 3). For O_3 and PAN, ZADV acts as a source at both the surface and in the PBL, but as a sink in the FT, suggesting that these species are transported from the FT to the PBL over Europe. ZADV is a source for all other species in the FT where they are advected away from the region. For reactive primary pollutants, chemistry (CHEM) is a sink at the surface over Europe since most of the emissions are close to the surface. It is also a sink for surface O_3 since O_3 chemical losses, including the reaction of O_3 with NO in the urban locations followed by HNO_3 formation, dominate over the photochemical production elsewhere. Similarly, CHEM is a sink for PAN due to the high temperatures that exist near the surface and drive PAN's thermal decomposition. For other secondary pollutants like HNO_3, CHEM is a source. On the other hand, within the PBL and the FT, O_3 is chemically produced by the transported precursors, while part of the NO_x transported from upwind is finally converted to HNO_3 and PAN (Table 3). SO_2 is also oxidized to sulfuric acid in all studied atmospheric layers. The results show that chemistry and aerosol processes

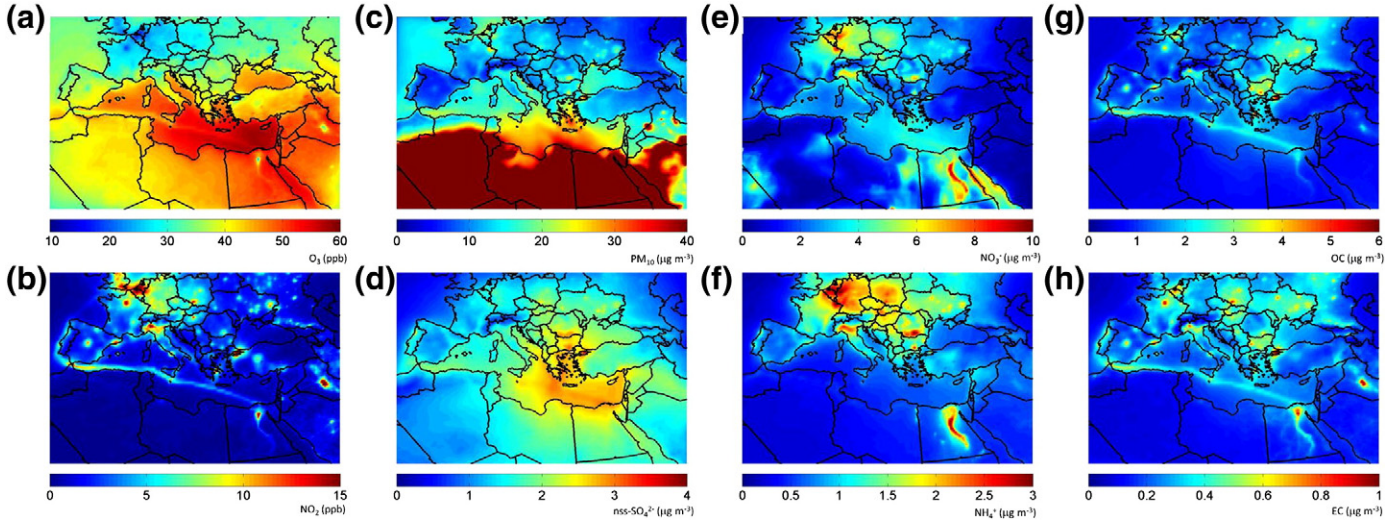

Fig. 6. Annual mean spatial distributions of computed surface O_3 (a), NO_2 (b), PM_{10} (c), nss-SO_4^{2-} (d), NO_3^- (e), NH_4^+ (f), OC (g) and EC (h). Units are ppb for O_3 and NO_2 and μg m^{-3} for all aerosol components.

Table 3
Budgets of major gaseous and particulate species over Europe at surface (lowest model layer) and within the Boundary layer (PBL that includes the surface layer) and free troposphere (FT) (units are Gg yr^{-1}). Negative values indicate a net loss from the altitude zone over Europe.

Species	ADV2	ZADV	CHEM	AERO	DDEP	CLDS	EMIS
SURFACE							
O_3	−536	4282	−3309		−34,405	288	
NO_x	−85	31	−666		−628	−235	15,975
PAN	−1	166	−143		−2600	24	
HNO_3	−72	87	741		−15,647	−16	
SO_2	−26	191	−37		−5312	−87	3509
nss-SO_4^{2-}	−28	87		50	−506	12	79
NH_4^+	−12	56		7	−361	−22	
NO_3^-	−63	117		−6340	−3983	−59	16,033
EC	−3	11		0	−59	−9	241
OC	−9	25		4	−190	−21	562
PM_{10}	−489	−454		−7107	−74,905	−423	124,197
PBL							
O_3	−37,925	6759	61,629		−34,405	2108	
NO_x	−2157	−413	−17,972		−628	−1157	23,057
PAN	−931	412	2715		−2600	−27	
HNO_3	−1865	−4246	12,634		−15,647	−2632	
SO_2	−2081	−757	−1238		−5312	−3816	13,456
nss-SO_4^{2-}	−1953	−412		1740	−506	1018	186
NH_4^+	−731	−177		2099	−361	−853	
NO_3^-	−2181	−482		−7492	−3983	−2056	16,424
EC	−138	−33		0	−59	−210	441
OC	−558	−123		555	−190	−576	914
PM_{10}	2225	−20,746		−22,787	−74,905	−2922	126,050
FT							
O_3	−24,378	−6564	12,221			−2524	
NO_x	498	408	−2334			1145	
PAN	−1323	−407	2070			24	
HNO_3	−3672	4222	−328			−1750	
SO_2	−421	752	−171			−483	
nss-SO_4^{2-}	−1626	436		247		796	
NH_4^+	−340	183		286		−140	
NO_3^-	−1378	487		534		28	
EC	−19	34		0		−29	
OC	−151	129		138		−170	
PM_{10}	−13,349	21,303		−2057		−9522	

are less effective in the FT compared to PBL where most of the emissions take place. Aerosol processes (AERO) act as a source for nss-SO_4^{2-}, NH_4^+ and OC over Europe both at the surface and within the PBL, while these processes remove NO_3^-. The contribution of AERO to EC is negligible compared to other species. Cloud processes (CLDS) that also include wet deposition lead to a net removal of most aerosol species except for nss-SO_4^{2-} due to its in-cloud production by the reaction of SO_2 and OH in clouds. Indeed, SO_2 is removed by the cloud processes both at the surface and within the PBL.

The calculated budgets over Europe in the boundary layer are compared to other estimates reported in the literature. In the present study, advection is calculated to be a sink for all inorganic aerosol components (Table 3), which implies that these pollutants are exported from the region, in agreement with Aan de Brugh et al. (2011). Both studies characterize advection as a sink for HNO_3 and SO_2, although it is almost an order of magnitude stronger in the present study. The impact of ZADV on pollutants compares well with the findings by Aan de Brugh et al. (2011), showing that convection is a sink for all aerosol species in the PBL. CHEM is calculated to be a sink for SO_2 and a source for HNO_3 (Table 3) in both studies. Regarding dry deposition (DDEP), at least 2 times higher deposition for nss-SO_4^{2-}, EC and OC is here calculated than by Aan de Brugh et al. (2011). Better agreement is found between DDEP estimates in the present study and those reported by Pozzer et al. (2012). Furthermore, the primary particulate emission fluxes (integrated for all model layers) used in our study are about 1.5 times lower while gaseous emissions are more than 2 times higher than those used in Aan de Brugh et al. (2011) and Pozzer et al. (2012). Overall, the above discussed differences between the model studies also reflect those in model horizontal and vertical resolutions, meteorology, the European domain definitions that the budgets are calculated for and therefore the emissions in these areas.

4. Conclusions

Major gaseous and particulate pollutant levels have been simulated using the WRF–CMAQ modeling system over Europe for 2008. The model results are compared with available observations from the EMEP stations, O_3 soundings, ship-borne O_3 and NO_2 observations in the western Mediterranean, tropospheric NO_2 VCDs from SCIAMACHY and AODs from AERONET.

Based on daily comparisons, surface O_3 levels are overestimated by 2% on a domain-mean basis, while underestimations are computed over western and north-western Europe (up to 30%) attributed to overestimated NO_x emissions. Observed vertical O_3 profiles are generally underestimated in the PBL by 10–20% which can be attributed to the observed overestimations of the tropospheric NO_2 VCDs (up to 40%), particularly over western Europe. Surface O_3 levels are overestimated by the model (up to ~65%) over southern Europe, with the highest overestimations over the western Mediterranean Sea, suggesting underestimated anthropogenic NO_x and overestimated biogenic NMVOC emissions, as well as uncertainties in the meteorological simulations. PM_{10} levels are underestimated by 10% to 30% in the southern and northeastern Europe, and overestimated by 7% in northwestern Europe while $PM_{2.5}$ levels are underestimated by 10% to 50%, with larger differences in southern and eastern Europe, suggesting underestimated particulate emissions. Larger differences are calculated for individual aerosol components, particularly for OC and EC. On the other hand, better agreements were found for the aerosol species, particularly in nss-SO_4^{2-}, over the urban areas of the eastern Mediterranean than other European regions and have been attributed to more detailed and finer resolution emission inventories for the eastern Mediterranean. Simulated AOD levels are on average 10% lower than the observations.

The results show a general north–south gradient around 40°N, with higher O_3 and PM_{10} levels in the south than in the north. For O_3, this pattern can be attributed to higher temperatures, solar radiation and transport of O_3 precursors into southern Europe. This region is also dominated by high PM_{10} levels due to the Saharan dust influence. Over the eastern Mediterranean, nss-SO_4^{2-} contributes significantly to the aerosol mass while NO_3^- and NH_4^+ are simulated to be high over the central and western Europe due to high anthropogenic emissions. NO_3^- levels are also high over the eastern Mediterranean sea due to the existence of the sea-salt particles that provide surface for the condensation of HNO_3 to produce NO_3^- particles. The OC and EC distributions clearly show the urban emission hot spots. Shipping routes in the Mediterranean are seen on O_3, OC and EC simulated distributions while not detected in SCIAMACHY retrievals. On the other hand, over continental Europe the distribution of NO_2 agrees reasonably well with NO_2 retrievals from SCIAMACHY observations. AOD levels are underestimated north of 40°N by 3% on average, due to underestimations in the anthropogenic emissions. Furthermore, south of 40°N, AODs are underestimated by 22% on average possibly due to underestimated natural and re-suspended dust emissions.

The budget calculations for the major gaseous and particulate species show that Europe acts as a net source region for most pollutants through vertical and horizontal transport, particularly in the upper troposphere, which is in agreement with earlier model studies. Our results show that surface, and more generally PBL O_3, is largely affected by transport from the upper troposphere. Uncertainties associated with emissions, area definitions and model spatial resolutions exist and should be considered in future studies.

Conflict of interest

The authors declare no conflict of interest.

Acknowledgments

This work has been performed in the frame of the EU-FP7 CityZen (Grant Agreement no. 212095), ECLIPSE (Grant Agreement no. 282688) and PARTHENO2N (PEOPLE-2009-RG, Grant Agreement no. 256391) projects. Regional emissions have been derived from the continental scale EMEP/INERIS inventory provided by G. Siour (LISA/IPSL/INERIS) and B. Bessagnet (INERIS). J. van Aardenene (EEA) is acknowledged for providing the CIRCE global anthropogenic emissions inventory.

Appendix A. Supplementary data

Supplementary data to this article can be found online at http://dx.doi.org/10.1016/j.scitotenv.2013.09.090.

References

Aan de Brugh JMJ, Schaap M, Vignati E, Dentener F, Kahnert M, Sofiev M, et al. The European aerosol budget in 2006. Atmos Chem Phys 2011;11:1117–39.
Appel KW, Chemel C, Roselle SJ, Francis XV, Hu R-M, Sokhi RS, et al. Examination of the Community Multiscale Air Quality (CMAQ) model performance over the North American and European domains. Atmos Environ 2012;53:142–55.
Basart S, Pay MT, Jorba O, Perez C, Jimenez-Guerrero P, Schulz M, et al. Aerosols in the CALIOPE air quality modeling system: evaluation and analysis of PM levels, optical depths and chemical composition over Europe. Atmos Chem Phys 2012;12:3363–92.
Becker S, Soukup JM, Sioutas C, Cassee FR. Response of human alveolar macrophages to ultrafine, fine, and coarse urban air pollution particles. Exp Lung Res 2003;29:29–44.
Burrows JP, Holzle E, Goede APH, Visser H, Fricke W. Sciamachy—scanning imaging absorption spectrometer for atmospheric cartography. Acta Astronaut 1995;35:445–51.
Byun D, Schere KL. Review of the governing equations, computational algorithms, and other components of the Models-3 Community Multiscale Air Quality (CMAQ) modeling system. Appl Mech Rev 2006;59:51–77.
California Air Resources Board (CARB). Speciation profiles used in CARB modeling. Sacramento, California: California Air Resources Board; 2007.
Carlton AG, Bhave PV, Napelenok SL, Edney EO, Sarwar G, Pinder RW, et al. Model representation of secondary organic aerosol in CMAQv4.7. Environ Sci Technol 2010;44:8553–60.
Colette A, Granier C, Hodneborg Q, Jakobs H, Mauruzu A, Nyiri A, et al. Air quality trends in Europe over the past decade: a first multi-model assessment. Atmos Chem Phys 2011;11:11657–78.
Dentener F, Kinne S, Bond T, Boucher O, Cofala J, Generoso S, et al. Emissions of primary and precursor gases in the years 2000 and 1750 prescribed data-sets for AeroCom. Atmos Chem Phys 2006;6:4321–44.
EC. Directive 2008/50/EC of the European Parliament and of the Council of 21 May 2008 on ambient air quality and cleaner air for Europe; 2008.
EC. Directive 2002/3/EC of the European Parliament and of the Council of 12 February 2002 relating to ozone in ambient air; 2002.
Engelstaedter S, Tegen I, Washington R. North African dust emissions and transport. Earth Sci Rev 2006;79:73–100.
European Commission (EC). Directive 2001/80/EC of the European Parliament and of the Council of 23 October 2001 on the limitation of emissions of certain pollutants into the air from large combustion plants; 2001.
Foley KM, Roselle SJ, Appel KW, Bhave PV, Pleim JE, Otte TL, et al. Incremental testing of the Community Multiscale Air Quality (CMAQ) modeling system version 4.7. Geosci Model Dev 2010;3:205–26.
Fowler D, Pilegaard K, Sutton MA, Ambus P, Raivonen M, Duyzer J, et al. Atmospheric composition change: ecosystems–atmosphere interactions. Atmos Environ 2009;43:5138–92.
Ginoux P, Chin M, Tegen I, Prospero JM, Holben B, Dubovik O, et al. Sources and distributions of dust aerosols simulated with the GOCART model. J Geophys Res 2001;106(D17):20255–73.
Gong SL. A parameterization of sea-salt aerosol source function for sub- and super-micron particles. Global Biogeochem Cycles 2003;17(4):1097. http://dx.doi.org/10.1029/2003GB002079.
Grell GA, Peckham SE, Schmitz R, McKeen SA, Frost G, Skamarock WC, et al. Fully coupled "online" chemistry within the WRF model. Atmos Environ 2005;39:6957–75.
Guenther A, Karl T, Harley P, Wiedinmyer C, Palmer PI, Geron C. Estimates of global terrestrial isoprene emissions using MEGAN (Model of Emissions of Gases and Aerosols from Nature. Atmos Chem Phys 2006;6:3181–210.
Han KM, Lee CK, Lee J, Kim J, Song CH. A comparison study between model-predicted and OMI-retrieved tropospheric NO_2 columns over the Korean peninsula. Atmos Environ 2011;45:2962–71.
Heue K-P, Richter A, Bruns M, Burrows JP, Frideburg Cv, Platt U, et al. Validation of SCIAMACHY tropospheric NO_2-columns with AMAXDOAS measurements. Atmos Chem Phys 2005;5:1039–51.
Huneeus N, Schulz M, Balkanski Y, Griesfeller J, Prospero J, Kinne S, et al. Global dust model intercomparison in AeroCom phase I. Atmos Chem Phys 2011;11:7781–816.
Im U, Kanakidou M. Impacts of East Mediterranean megacity emissions on air quality. Atmos Chem Phys 2012;12:6335–55.
Im U, Markakis K, Poupkou A, Melas D, Unal A, Gerasopoulos E, et al. The impact of temperature changes on summer time ozone and its precursors in the Eastern Mediterranean. Atmos Chem Phys 2011;11:3847–64.
Im U, Markakis K, Kocak M, Gerasopoulos E, Daskalakis N, Mihalopoulos N, et al. Summertime aerosol chemical composition in the Eastern Mediterranean and its sensitivity to temperature. Atmos Environ 2012;50:164–73.
Im U, Incecik S, Guler M, Tek A, Topcu S, Unal YS, et al. Analysis of surface ozone and nitrogen oxides at urban, semi-rural and rural sites in Istanbul, Turkey. Sci Total Environ 2013;443:920–31.
Inness A, Baier F, Benedetti A, Bouarar I, Chabrillat S, Clark H, et al. The MACC reanalysis: an 8 yr data set of atmospheric composition. Atmos Chem Phys 2013;13:4073–109.
Intergovernmental Panel on Climate Change (IPCC). Climate change 2007: the physical science basis. Cambridge University Press; 2007.
Karanasiou A, Moreno T, Amato F, Lumbreras J, Narros A, Borge R, et al. Road dust contribution to PM levels—evaluation of the effectiveness of street washing activities by means of positive matrix factorization. Atmos Environ 2011;45:2193–201.
Katragkou E, Zanis P, Kioutsioukis I, Tegoulias I, Melas D, Kruger BC, et al. Future climate change impacts on summer surface ozone from regional climate-air quality simulations over Europe. J Geophys Res 2011;116:D22307. http://dx.doi.org/10.1029/2011JD015899.
Kelly JT, Bhave PV, Nolte CG, Shankar U, Foley KM. Simulating emissions and chemical evolution of coarse sea-salt particles in the Community Multiscale Air Quality (CMAQ) model. Geosci Model Dev 2010;3:257–73.
Koçak M, Theodosi C, Zarmpas P, Im U, Bougiatioti A, Yenigun O, et al. Particulate matter (PM_{10}) in Istanbul: origin, sources and potential impact on surrounding regions. Atmos Environ 2011;45:6891–900.
Kukkonen J, Olsson T, Schultz DM, Baklanov A, Klein T, Miranda AI, et al. A review of operational, regional-scale, chemical weather forecasting models in Europe. Atmos Chem Phys 2012;12:1–87.
Malm WC, Sisler JF, Huffman D, Eldred RA, Cahill TA. Spatial and seasonal trends in particle concentration and optical extinction in the United States. J Geophys Res 1994;99(D1):1347–70.
Markakis K, Poupkou A, Melas D, Zerefos C. A GIS based anthropogenic PM10 emission inventory for Greece. Atmos Pollut Res 2010;1(2):71–81.
Markakis K, Im U, Unal A, Melas D, Yenigun O, Incecik S. Compilation of a GIS based high spatially and temporally resolved emission inventory for the Greater Istanbul Area. Atmos Pollut Res 2012;3:112–25.
Matthias V. The aerosol distribution in Europe derived with the Community Multiscale Air Quality (CMAQ) model: comparison to near surface in situ and sunphotometer measurements. Atmos Chem Phys 2008;8:5077–97.
Megaritis AG, Fountoukis C, Charalampidis PE, Pilinis C, Pandis SN. Response of fine particulate matter to changes of emissions and temperature in Europe. Atmos Chem Phys 2013;13:3423–43.
Mitsakou C, Kallos G, Papantoniou N, Spyrou C, Solomos S, Astitha M, et al. Saharan dust levels in Greece and received inhalation doses. Atmos Chem Phys 2008;8:7181–92.
Myriokefalitakis S, Tsigaridis K, Mihalopoulos N, Sciare J, Nenes A, Kawamura K, et al. In-cloud oxalate formation in the global troposphere: a 3-D modeling study. Atmos Chem Phys 2011;11:5761–82.
Nel A. Air pollution-related illness: effects of particles. Science 2005;308:804–6.
Nenes A, Pandis SN, Pilinis C. ISORROPIA: a new thermodynamic equilibrium model for multiphase multicomponent inorganic aerosols. Aquat Geochem 1998;4(1):123–52.
Nicolas J, Chiari M, Crespo J, Orellana IG, Lucarelli F, Nava S, et al. Quantification of Saharan and local dust impact in an arid Mediterranean area by the positive matrix factorization (PMF) technique. Atmos Environ 2008;42:8872–82.
Olivier JGJ, Berdowski JJM, Bakker JAHWJ, Visschedijk AJH, Bloos J-PJ. Applications of EDGAR. Including a description of EDGAR 3.0: reference database with trend data for 1970–1995. Bilthoven: RIVM; 2001 (RIVM report no. 773301 001/NOP report no. 410200 051 (available at http://www.rivm.nl/bibliotheek/)).
Otte TL, Pleim JE. The Meteorology–Chemistry Interface Processor (MCIP) for the CMAQ modeling system: updates through MCIPv3.4.1. Geosci Model Dev 2010;3:243–56.
Paraskevopoulou D, Gerasopoulos E, Liakakou E, Gratsea M, Zarmpas P, Theodosi C, et al. Optical properties of aerosols over Athens, Greece, and their relation with chemical composition. 11th International Conference on Meteorology, Climatology and Atmospheric Physics, COMECAP 2012, Athens 30 May–1 June 2012; 2012.
Pateraki St, Assimakopoulos VD, Bougiatioti A, Kouvarakis G, Mihalopoulos N, Vasilakos Ch. Carbonaceous and ionic compositional patterns of fine particles over an urban Mediterranean area. Sci Total Environ 2012;424:251–63.
Pay MT, Piot M, Jorba O, Gasso S, Goncavles M, Basart S, et al. A full year evaluation of the CALIOPE_EU air quality modeling system over Europe for 2004. Atmos Environ 2010;44:3322–42.
Pozzer A, de Meij A, Pringle KJ, Tost H, Doering UM, van Aardanne J, et al. Distributions and regional budgets of aerosols and their precursors simulated with the EMAC chemistry-climate model. Atmos Chem Phys 2012;12:961–87.
Querol X, Alastuey A, Pey J, Cusack M, Pérez N, Mihalopoulos N, et al. Variability in regional background aerosols within the Mediterranean. Atmos Chem Phys 2009;9:4575–91.
Ramanathan V, Crutzen PJ, Kiehl JT, Rosenfeld D. Aerosols, climate, and the hydrological cycle. Science 2001;294:2119–24.

Richter A, Burrows JP. Tropospheric NO_2 for GOME measurements. Adv Space Res 2002;29(11):1673–83.
Richter A, Burrows JP, Nüß H, et al. Increase in tropospheric nitrogen dioxide over China observed from space. Nature 2005;437:129–32.
Roy B, Mathur R, Gilliland AB, Howard SC. A comparison of CMAQ-based aerosol properties with IMPROVE, MODIS, and AERONET data. J Geophys Res 2007;112:D14301.
Russell A, Dennis R. NARSTO critical review of photochemical models and modeling. Atmos Environ 2000;34(12–14):2283–324.
Schembari C, Cavalli F, Cuccia E, Hjorth J, Calzolai G, Pérez N, et al. Impact of a European directive on ship emissions on air quality in Mediterranean Harbours. Atmos Environ 2012;61:661–9.
Shi C, Fernando HJS, Wang Z, An X, Wu Q. Tropospheric NO_2 columns over East Central China: comparisons between SCIAMACHY measurements and nested CMAQ simulations. Atmos Environ 2008;42:7165–73.
Simpson D, Fagerli H, Jonson JE, Tsyro S, Wind P, Tuovinen J-P. Transboundary acidification, eutrophication and ground level ozone in Europe. PART I. Unified EMEP model description. EMEP Report 1/2003. Norwegian Meteorological Institute; 2003. [ISSN 0806-4520, 104 pp.].
Skamarock WC, Klemp JB. A time-split non-hydrostatic atmospheric model. J Comput Phys 2008;227:3465–85.
Tang Y, Huang H-C, Lee P, Lu S, McQueen JT, Lin H-M, et al. A case study using the CMAQ coupling with GFS-GOCART dust lateral boundary conditions. 7th Annual Community Modeling & Analysis System (CMAS) Conference, October 6–8, Chapel Hill, NC, USA; 2008.
Theodosi C, Im U, Bougiatioti A, Zarmpas P, Yenigun O, Mihalopoulos N. Aerosol chemical composition over Istanbul. Sci Total Environ 2010;408(12):2482–91.
Theodosi C, Grivas G, Zarmpas P, Chaloulakou A, Mihalopoulos N. Mass and chemical composition of size-segregated aerosols (PM_1, $PM_{2.5}$ and PM_{10}) over Athens, Greece: local versus regional sources. Atmos Chem Phys 2011;11:11895–911.
Vrekoussis M, Richter A, Hilboll A, Burrows JP, Gerasopoulos E, Lelieveld J, et al. Economic crisis detected from space: air quality observations over Athens/Greece. Geophys Res Lett 2013;40. http://dx.doi.org/10.1002/grl.50118.
Wiedinmyer C, Akagi SK, Yokelson RJ, Emmons LK, Al-Saadi JA, Orlando JJ, et al. The fire inventory from NCAR (FINN): a high resolution global model to estimate the emissions from open burning. Geosci Model Dev 2011;4:625–41.
Wilson RC, Fleming ZL, Monks PS, Clain G, Henne S, Konovalov IB, et al. Have primary emission reduction measures reduced ozone across Europe? An analysis of European rural background ozone trends 1996–2005. Atmos Chem Phys 2012;12:437–54.
World Meteorological Organization (WMO). WMO statement on the status of the global climate in 2002, WMO No. 949; 2003.
Yardwood G, Rao S, Yocke M, Whitten GZ. Updates to the carbon bond chemical mechanism: CB05. Final report to the US EPA, RT-0400675, December 8, 2005; 2005.
Zyrichidou I, Koukouli ME, Balis DS, Katragkou E, Melas D, Poupkou A, et al. Satellite observations and model simulations of tropospheric NO_2 columns over south-eastern Europe. Atmos Chem Phys 2009;9:6119–34.